Noise considerations of three-point water-fat separation imaging methods

Zhifei Wen[a)]
Department of Physics, Stanford University, Stanford, California 94305 and Department of Radiology, Stanford University, Stanford, California 94305

Scott B. Reeder[b)] and Angel R. Pineda[c)]
Department of Radiology, Stanford University, Stanford, California 94305

Norbert J. Pelc
Department of Radiology, Stanford University, Stanford, California 94305 and Department of Bioengineering, Stanford University, Stanford, California 94305

(Received 19 November 2007; revised 29 April 2008; accepted for publication 4 June 2008; published 16 July 2008)

Separation of water from fat tissues in magnetic resonance imaging is important for many applications because signals from fat tissues often interfere with diagnoses that are usually based on water signal characteristics. Water and fat can be separated with images acquired at different echo time shifts. The three-point method solves for the unknown off-resonance frequency together with the water and fat densities. Noise performance of the method, quantified by the effective number of signals averaged (NSA), is an important metric of the water and fat images. The authors use error propagation theory and Monte Carlo simulation to investigate two common reconstructive approaches: an analytic-solution based estimation and a least-squares estimation. Two water-fat chemical shift (CS) encoding strategies, the symmetric $(-\theta,0,\theta)$ and the shifted $(0,\theta,2\theta)$ schemes are studied and compared. Results show that NSAs of water and fat can be different and they are dependent on the ratio of intensities of the two species and each of the echo time shifts. The NSA is particularly poor for the symmetric $(-\theta,0,\theta)$ CS encoding when the water and fat signals are comparable. This anomaly with equal amounts of water and fat is analyzed in a more intuitive geometric illustration. Theoretical prediction of NSA matches well with simulation results at high signal-to-noise ratio (SNR), while deviation arises at low SNR, which suggests that Monte Carlo simulation may be more appropriate to accurately predict noise performance of the algorithm when SNR is low.
[DOI: 10.1118/1.2952644]

Key words: MRI, water-fat separation, three point, NSA, CRB, simulation

I. INTRODUCTION

Magnetic resonance (MR) imaging is a powerful tool in medical diagnosis. MR signals are derived from the total proton nuclear magnetization, most of which comes from protons in water and fat tissues. The image from the water component is generally more important for detection and characterization of pathologies, while the fat component may obscure underlying abnormalities. Water-fat separation imaging solves this problem by producing separate water and fat images from multiple images acquired at different time shifts from the spin echo. In the original approach,[1] the main magnetic field is assumed to be homogeneous and known, and the spectral width of each component is assumed to be negligible. The MR signal at an echo time shift t_n is

$$S_n = \rho_w + \rho_f e^{i2\pi\Delta f t_n}, \tag{1}$$

where ρ_w is the on-resonance water component and ρ_f is the fat component that precesses at a chemical shift frequency Δf. Two MR signals are obtained at echo time shifts t_0 and t_1 chosen such that

$$\begin{aligned} 2\pi\cdot\Delta f\cdot t_0 &= 2k\pi, \\ 2\pi\cdot\Delta f\cdot t_1 &= (2k+1)\pi, \end{aligned} \tag{2}$$

where k is an integer. The two acquired images are then

$$\begin{aligned} S_0 &= \rho_w + \rho_f, \\ S_1 &= \rho_w - \rho_f, \end{aligned} \tag{3}$$

and water and fat images can be calculated as

$$\begin{aligned} \rho_w &= \frac{1}{2}(S_0 + S_1), \\ \rho_f &= \frac{1}{2}(S_0 - S_1). \end{aligned} \tag{4}$$

However, this simple approach fails in practice where the field is inhomogeneous. The off-resonance frequency ψ (due to the inhomogeneous field) causes an additional phase term in the MR signal, so that

$$S_n = (\rho_w + \rho_f e^{i2\pi\Delta f t_n})e^{i2\pi\psi t_n}, \quad (5)$$

leading to erroneous decomposition into water and fat if Eq. (4) is used.

In order to remove the phase errors, Glover *et al.*[2,3] used three echo time shifts that have a constant water-fat phase incremental angle between adjacent echo time shifts

$$\theta = 2\pi \cdot \Delta f \cdot \Delta t, \quad (6)$$

where $\Delta t = t_{n+1} - t_n$. From the MR signals, algebraic solutions for ρ_w and ρ_f can be found to estimate the water and fat components. Meanwhile, the noise from the MR signals will propagate into the estimation of water and fat. How the estimation is affected by the signal noise was presented in Ref. 3 as a plot of $\mathrm{NSA_{eff}}$ (effective number of signals averaged) versus θ for water-fat chemical shift (CS) encoding $(-\theta, 0, \theta)$ under the assumption that only one of the two species dominates the other ($\rho_w \gg \rho_f$ or $\rho_f \gg \rho_w$).

Areas where water and fat have comparable signal magnitudes, e.g., interfaces between water and fat, and tissues with mixed contents (e.g., fatty liver) can be of substantial clinical interest. How the water/fat composition affects the noise behavior of the water-fat separation methods has not been fully studied. Besides the symmetric water-fat CS encoding $(-\theta, 0, \theta)$, other encodings, such as $(0, \theta, 2\theta)$ (Refs. 3 and 4) and $(\theta_0, \theta_0+\theta, \theta_0+2\theta)$,[5] have been explored. However, the noise performances of these methods have not been systematically studied. Recently, Reeder *et al.*[6] proposed a new approach for multipoint water-fat separation. In this method, water, fat, and the field map are unknown parameters in the signal model and they are estimated by an iterative nonlinear least-squares (LS) fit to the acquired MR signals.

In order to optimize the imaging acquisition parameters and reconstruction algorithms to improve the image quality and shorten computational time, a better understanding on how echo time shifts, water/fat composition, and reconstruction methods influence the number of signals averaged (NSA) is needed. In this article, we first review two computation methods, the analytic and the LS approaches. We then study their noise performance using noise propagation theory and Monte Carlo simulations for two CS encodings, the symmetric $(-\theta, 0, \theta)$ and the shifted $(0, \theta, 2\theta)$ approaches. The two methods and the two encodings are compared at both high and low noise levels. A special example is presented with geometric illustration to help understand the results.

II. METHODS

II.A. Analytical solutions

A commonly used water-fat separation method[2,3] utilized a symmetric three-point encoding in which three images are collected at three evenly spaced time points $(-\Delta t, 0, \Delta t)$,

$$S_{-1} = (\rho_w + \rho_f e^{-i\theta})e^{-i\phi},$$

$$S_0 = \rho_w + \rho_f, \quad (7)$$

$$S_1 = (\rho_w + \rho_f e^{i\theta})e^{i\phi},$$

where $\phi = 2\pi \cdot \psi \cdot \Delta t$ is the common CS incremental angle due to the off-resonance frequency (field map). The solution for ρ_w and ρ_f to these equations given in Ref. 3 is

$$\rho_{w,f} = \frac{S_0}{2} \pm \frac{1}{2}\sqrt{S_0^2 - 2(S_0^2 - S_1 S_{-1})/(1 - \cos\theta)}, \quad (8)$$

with the species of higher abundance taking the plus sign. Species recognition in analytic methods can be achieved by assuming certain behaviors of the field map such as a slowly varying map,[7] or using information from nearby pixels to choose between two possible solutions, leaving the noise performance of the solutions themselves unaffected. Whether water and fat can be easily identified depends on whether the phase map can be unwrapped, which in turn depends on the noise level and phase unwrapping techniques.[8] In order to focus on the intrinsic statistical effectiveness of the estimation methods, we assume that water and fat are always correctly recognized. For simplicity and without loss of generality, water is assumed to be more abundant than fat, i.e., $\rho_w > \rho_f$, in all the following analytic solutions. Since the noise in the source images is independent Gaussian noise[9] with a small variance σ_0^2 in both the I and Q channels, the variances of ρ_w and ρ_f can be approximated as

$$\sigma_{w,f}^2 \approx \sum_n \left|\frac{\partial \rho_{w,f}}{\partial S_n}\right|^2 \sigma_0^2. \quad (9)$$

In order to quantify the noise performance, the signal-to-noise ratio (SNR)-equivalent $\mathrm{NSA_{eff}}$ is defined in Ref. 3,

$$\mathrm{NSA_{eff}} = \frac{\sigma_0^2}{\sigma_\rho^2}. \quad (10)$$

From Eqs. (8) and (9), the NSAs for ρ_w and ρ_f can be derived

$$\begin{aligned}\mathrm{NSA}_w &= \sigma_0^2/\sigma_w^2 = 2(R_{\mathrm{wf}} - 1)^2(1 - \cos\theta)^2/[(2\cos^2\theta \\ &\quad + 1)R_{\mathrm{wf}}^2 + 6\cos\theta \cdot R_{\mathrm{wf}} + 3], \\ \mathrm{NSA}_f &= \sigma_0^2/\sigma_f^2 = 2(R_{\mathrm{wf}} - 1)^2(1 - \cos\theta)^2/[(2\cos^2\theta + 1) \\ &\quad + 6\cos\theta \cdot R_{\mathrm{wf}} + 3R_{\mathrm{wf}}^2],\end{aligned} \quad (11)$$

where $R_{\mathrm{wf}} = \rho_w/\rho_f$ is the water to fat ratio and σ_w^2 and σ_f^2 are the variance in ρ_w and ρ_f, respectively. It is evident in Eqs. (11) that the NSAs of both water and fat depend on the water to fat ratio R_{wf} as well as the water-fat CS encoding angle θ. In fact, Eqs. (11) predict that when $\rho_w = \rho_f$ ($R_{\mathrm{wf}} = 1$) the NSAs are zero for all values of θ except for $\theta = \pi$. When there is only water ($R_{\mathrm{wf}} \gg 1$), Eqs. (11) can be simplified to

$$\mathrm{NSA}_w = \frac{\sigma_0^2}{\sigma_w^2} = \frac{2(1-\cos\theta)^2}{1+2\cos^2\theta},$$
$$\mathrm{NSA}_f = \frac{\sigma_0^2}{\sigma_f^2} = \frac{2(1-\cos\theta)^2}{3}. \quad (12)$$

The NSA for water has a maximum of 3 at $\theta=2\pi/3$ and is equal to 8/3 at $\theta=\pi$, as previously given by Glover *et al.*[3] The NSA for fat increases monotonically from 0 to 8/3 as θ goes from 0 to π.

As a generalization of Glover's encoding scheme, Xiang *et al.*[5] proposed to use echo time shifts of $(t_0, t_0+\Delta t, t_0+2\Delta t)$, which allowed increased flexibility in MR imaging. The acquired signals in this case are

$$S_1 = (\rho_w + \rho_f e^{i\theta_0})e^{i\phi_0},$$
$$S_2 = (\rho_w + \rho_f e^{i(\theta_0+\theta)})e^{i(\phi_0+\phi)}, \quad (13)$$
$$S_3 = (\rho_w + \rho_f e^{i(\theta_0+2\theta)})e^{i(\phi_0+2\phi)},$$

where $\theta_0=2\pi\Delta f\cdot t_0$ and $\phi_0=2\pi\psi\cdot t_0$. Since the number of unknown parameters (ρ_w, ρ_f, ψ) is less than the number of equations (in real numbers), there can be multiple solutions for ρ_w and ρ_f. With no noise, these solutions are all consistent and mathematically exact. When noise is considered, the solution may exhibit different responses to noise. The solution provided by Xiang *et al.*[5] is

$$|\rho_{w,f}| = \left|\frac{1}{2}\left[S_2 \pm \frac{\sqrt{(e^{i\theta}+1)^2S_2^2 - 4e^{i\theta}S_1S_3}}{e^{i\theta}-1}\right]\right|, \quad (14)$$

and its noise performance can also be predicted with error propagation as shown in Eq. (9).

II.B. Numerical solutions

II.B.1. The Cramer–Rao bound

The goal of the water-fat separation method is to estimate unknown parameters (ρ_w, ρ_f, and ψ) using measured MR signals. As the problem is overdetermined, there can be a variety of estimation methods whose merit can be judged by two criteria: bias and variance. For all unbiased estimations, the Cramer–Rao bound (CRB) is the lower bound on the variance, which can be asymptotically achieved by the maximum likelihood estimation (MLE). The MLE with Gaussian noise is the LS estimation. Pineda *et al.*[10] calculated the CRB for the three point method and showed that it could be achieved by the LS estimation implemented by Reeder and Yu.[6,11,12] Here, we compare their work with the noise performance of the analytic methods to show the difference between the two reconstruction methods with the data simulated with the same CS encoding scheme.

II.B.2. Linear LS estimation

If three MR images are acquired at (t_1, t_2, t_3),

$$S_n = (\rho_w + \rho_f e^{i2\pi\Delta f t_n})e^{i2\pi\psi t_n},$$
$$n = 1,2,3, \quad (15)$$

the estimation of ρ_w and ρ_f is nonlinear unless the field map ψ is known and ρ_w and ρ_f are allowed to be complex numbers. Then the above equations can be rewritten in a matrix form

$$\begin{bmatrix} S_1' \\ S_2' \\ S_3' \end{bmatrix} = \begin{bmatrix} S_1 e^{-i2\pi\psi\cdot t_1} \\ S_2 e^{-i2\pi\psi\cdot t_2} \\ S_3 e^{-i2\pi\psi\cdot t_3} \end{bmatrix} = \begin{bmatrix} 1 & e^{-i2\pi\Delta f\cdot t_1} \\ 1 & e^{-i2\pi\Delta f\cdot t_2} \\ 1 & e^{-i2\pi\Delta f\cdot t_3} \end{bmatrix} \begin{bmatrix} \rho_w \\ \rho_f \end{bmatrix}. \quad (16)$$

Since each S_n' is a linear function of ρ_w and ρ_f, linear LS estimation can be used to estimate ρ_w and ρ_f. Reference 6 shows the estimated real and imaginary components of the computed water and fat signals have the same variance leading to

$$\mathrm{NSA}_{\rho(R,I)} = 3 - \frac{\sin^2\frac{3\theta}{2}}{3\sin^2\frac{\theta}{2}}. \quad (17)$$

Because it is difficult to display complex numbers in a MR image, magnitudes $|\rho_w|$ and $|\rho_f|$ are often used. If noise in the real and imaginary components is uncorrelated and small compared to $|\rho_w|$ and $|\rho_f|$, the variances of $|\rho_w|$ and $|\rho_f|$ are equal to $\sigma^2_{\rho(R,I)}$. With these assumptions, the NSA for the magnitudes of water and fat are the same as in Eq. (17).

II.B.3. Nonlinear LS estimation

When the field map is unknown, the problem is no longer linear. In Reeder's iterative algorithm,[6] the field map is assumed to be known in each iteration and the field map is updated for the next iteration based on discrepancies between the predicted signals and the original signals. By using a region growing process and information from neighboring pixels, an initial guess close to the true field map can be achieved in order to make the pixel based separation algorithm more reliable and practical.[12,13] Iterations are repeated until changes of the fitting parameters are small or the maximum number of iterations has been reached. Stringent stopping criteria were used in our simulations so that the results could be comparable to theoretically predicted limits which can only be obtained with an infinite number of iterations. In real applications stopping criteria can be relaxed to save computation time.

II.C. Monte Carlo simulation

Monte Carlo simulation was used to verify the NSAs derived from Eq. (9) for the analytic solutions and the NSAs derived from the CRB for the numerical solution. Simulated signals were generated based on the signal models from Eqs. (7) and (13) for a range of water-to-fat ratios (total signal normalized to $\rho_w+\rho_f=1$) and various CS encoding strategies. Zero mean Gaussian noise with standard deviation σ was added to the real and imaginary components of the signals, which were then sent to the analytic and iterative LS solutions for estimation of water and fat. This process was per-

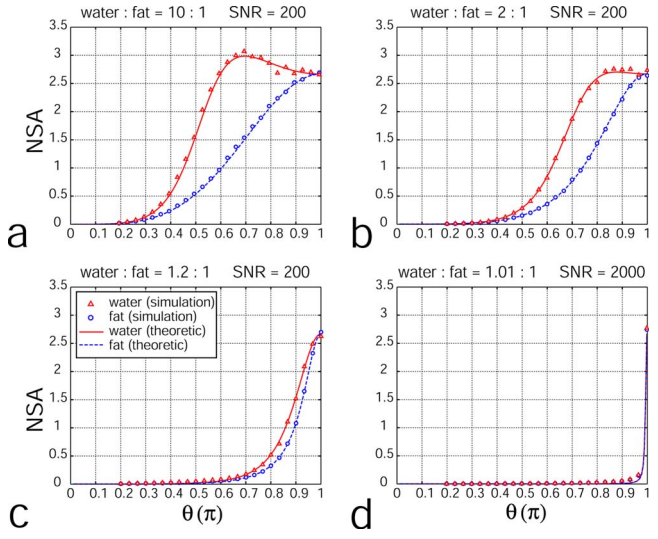

FIG. 1. Theoretically predicted NSA vs θ curves with Monte Carlo simulation results for MR signals with CS encoding of $(-\theta,0,\theta)$. The analytic solution was used to estimate water and fat. The water-to-fat ratios were (a) $R_{wf}=10$, (b) $R_{wf}=2$, (c) $R_{wf}=1.2$, and (d) $R_{wf}=1.01$. Data points of triangles and circles indicate NSAs for magnitudes of water and fat.

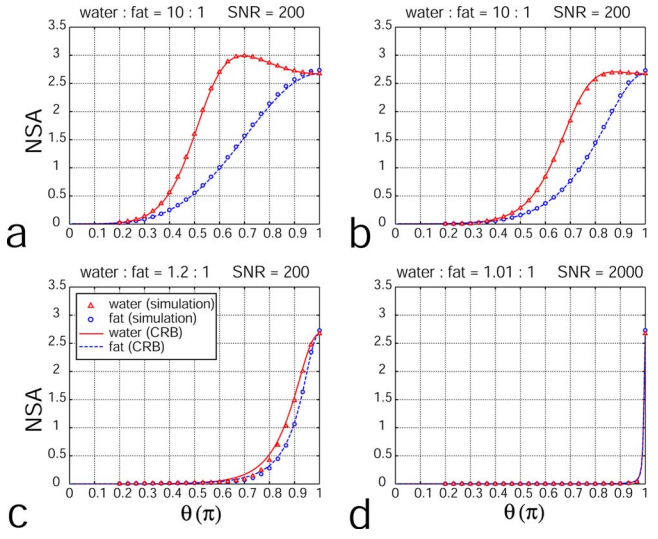

FIG. 2. NSA vs θ curves given by the CRB with Monte Carlo simulation results. MR signals were generated with the CS encoding of $(-\theta,0,\theta)$ and the LS solution was used to estimate water and fat. The water-to-fat ratios were (a) $R_{wf}=10$, (b) $R_{wf}=2$, and (c) $R_{wf}=1.2$, and (d) $R_{wf}=1.01$.

formed 5000 times for each choice of R_{wf} and encoding and the estimated quantities were computed. The NSAs were calculated as σ^2 divided by the measured variance of ρ_w or ρ_f.

Low noise ($\sigma \leq 1/200, \mathrm{SNR} \geq 200$) was first used to confirm the agreement with the simulation results and theoretically predicted NSA. For the analytic method, the approximation in Eq. (9) becomes less accurate with large noise. For the iterative method, large noise can cause deviation of the performance of MLE from the CRB because MLE may not achieve CRB when the asymptotic conditions (small errors) are not satisfied.[14] Furthermore, large noise may cause convergence to an erroneous solution (local minimum) or even nonconvergence. Simulation at a more realistic noise level (SNR=25) was also performed to show how NSA performance could be affected with noisy data.

III. RESULTS

III.A. High SNR simulation (SNR≥200)

III.A.1. $(-\theta,0,\theta)$ *CS encoding*

Figure 1 shows the NSAs of water and fat as functions of θ with CS encoding $(-\theta,0,\theta)$ at four water-to-fat ratios, 10, 2, 1.2, and 1.01. The analytic solution in Eq. (8) was used to calculate the water and fat components. Thus the predicted NSAs were given by Eqs. (11) and plotted as solid lines. The data points are Monte Carlo simulation results based on the analytic solution. A SNR of 200 was used in all water-to-fat ratios except for $R_{wf}=1.01$, where a higher SNR of 2000 was used to ensure correct choice of water or fat. In the presence of noise, solutions for water and fat were in complex numbers, and their magnitudes were taken in computing NSAs. The NSAs of simulations agreed well with the theoretical predictions. The NSAs of water and fat not only depended on θ, but also on the water-to-fat ratio. If one species dominated, as in Fig. 1(a), the NSA of the dominant species was much higher than that of the less abundant species. The maximum NSA occurred at $\theta=2\pi/3$, with uniform spacing of three phase encoding angles around the full circle. The NSAs for both species and the difference between them decreased as the water-to-fat ratio increased, as shown in Figs. 1(b)–1(d). When water and fat were almost equal [Fig. 1(d)], for any θ not equal to π, the NSAs were close to zero, in accordance to Eqs. (11). When $\theta=\pi$, NSAs of both water and fat stayed about 2.7, the same value as in other water-to-fat ratios at $\theta=\pi$. This striking loss of NSA when water and fat are almost equal and $\theta \neq \pi$ is discussed in detail below and a graphical explanation is presented.

Figure 2 shows the NSA curves for water and fat with the same CS encoding and water-to-fat ratios as used in Fig. 1. Smooth NSA curves are the CRB, and Reeder's implementation of the LS estimation was used in Monte Carlo simulations. Simulation results matched the CRB well in most cases, except for $\theta<0.8\pi$ in Fig. 2(c) when the NSAs were slightly lower than the CRB curves. The discrepancies could have been caused by nonconvergence of fitting when water and fat were similar at small θ.

Comparison of Figs. 1 and 2 shows that there is no distinguishable difference between the predicted NSAs of the analytic solution and the CRB. It was somewhat surprising that the analytic solution at CS encoding $(-\theta,0,\theta)$ had the same NSA performance as the lower bound given by the CRB, since the analytic solution was not based on the MLE. This raises the question whether the analytic solution was biased. Equation (18) shows that the mean square error $(\sigma^2_{\mathrm{MSE}})$ has two contributing sources, the variance $\mathrm{Var}(\rho)$ and the bias $(\bar{\rho}-\rho_t)$, where ρ_k is the estimate, $\bar{\rho}$ is the mean, and ρ_t is the true value

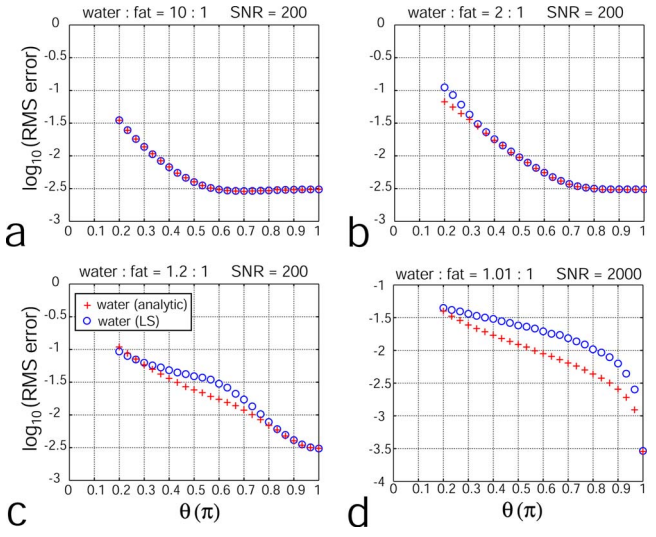

FIG. 3. Simulation results of the RMS error vs θ of the analytic and iterative solutions with CS encoding of $(-\theta,0,\theta)$ and water-to-fat ratios at (a) $R_{wf}=10$, (b) $R_{wf}=2$, (c) $R_{wf}=1.2$, and (d) $R_{wf}=1.01$.

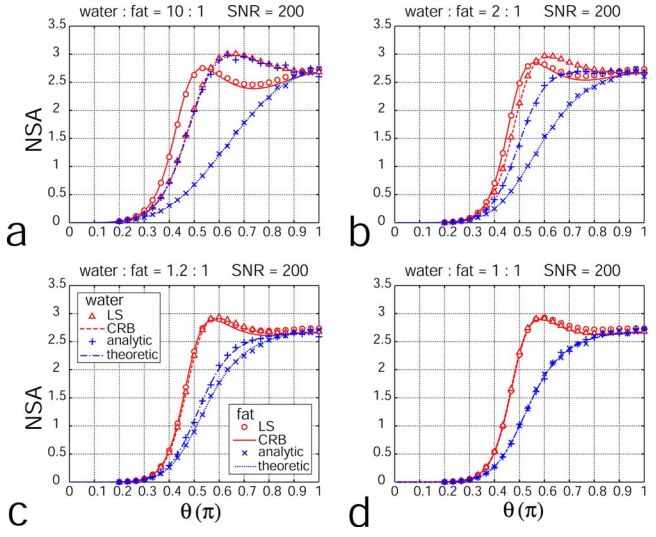

FIG. 4. Comparison of NSAs obtained with analytic and iterative (LS) solutions. Predicted NSAs are plotted as smooth curves with data points obtained with Monte Carlo simulations. The CS encoding was $(0,\theta,2\theta)$ and the water-to-fat ratios were (a) $R_{wf}=10$, (b) $R_{wf}=2$, (c) $R_{wf}=1.2$, and (d) $R_{wf}=1$.

$$\sigma^2_{\mathrm{MSE}}=\frac{1}{n}\sum_{k=1}^{n}(\rho_k-\rho_t)^2=\frac{1}{n}\sum_{k=1}^{n}[(\rho_k-\bar{\rho})+(\bar{\rho}-\rho_t)]^2$$

$$=\frac{1}{n}\sum_{k=1}^{n}(\rho-\bar{\rho})^2+(\bar{\rho}-\rho_t)^2=\mathrm{Var}(\rho)+(\bar{\rho}-\rho_t)^2. \quad (18)$$

With the assumption that the LS estimation is unbiased or its bias due to nonideal implementation can be neglected in our application, comparing the root-mean-square (RMS) errors of the analytic and numerical solutions would manifest whether there is significant bias in the analytic solution.

Figure 3 shows the RMS errors of the water estimate in the simulations in Figs. 1 and 2. RMS errors for fat were very similar to those for water, and therefore they are not shown here. No difference was observed in the RMS errors between the analytic and numerical LS solutions when there is a dominant species [Fig. 3(a)]. In Fig. 3(b), for θ less than $\sim 0.3\pi$, the RMS errors of the analytic solution were slightly less than those of the LS solution; for θ larger than $\sim 0.3\pi$, the difference was negligible. When $R_{wf}=1.2$, the RMS errors of both methods were similar for small θ and they decreased as θ increased, as shown in Fig. 3(c). However, the RMS errors for the analytic solution decreased more rapidly than those of the errors for the LS solution starting from $\theta=0.3\pi$. For $\theta>0.8\pi$, the errors of both solutions became similar again. At $R_{wf}=1.01$, the difference in RMS errors was more pronounced: the errors of the analytic solution were consistently less than those of the LS solution except when $\theta=\pi$ [Fig. 3(d)]. This discrepancy in errors of the two solutions may have resulted from incorrect convergences or erroneous assignment of water and fat in the LS solution when the amounts of water and fat were comparable. This effect can be avoided in the analytic solution when the correct sign of the solution in Eq. (8) was chosen with the help of species recognition. By comparing RMS errors of the two solutions at large θ, we were not able to show that the analytic-solution-based estimation was more biased than the LS based estimation.

III.A.2. $(0,\theta,2\theta)$ phase encoding

Figure 4 shows the NSAs of water and fat for MR signals acquired using the $(0,\theta,2\theta)$ encoding strategy at four water-to-fat ratios. For the analytic solution given by Eq. (14), the NSA performance was predicted with Eq. (9). For the iterative solution, NSAs were predicted by the CRB and Reeder's implementation of the LS estimation was used in Monte Carlo simulations. Simulation results matched the predictions well. NSAs for water decreased as the water component decreased, while the NSAs for fat increased as the fat component increased. Comparison of NSAs obtained from the analytic solution and the iterative solution shows that NSAs with the $(0,\theta,2\theta)$ CS encoding were consistently higher than those with the $(-\theta,0,\theta)$ encoding. For instance, at $\theta=\pi/2$, the water and fat NSAs were 2.0 and 0.7 with $(0,\theta,2\theta)$ in Fig. 4(a), as opposed to 1.5 and 0.5 $(-\theta,0,\theta)$ in Fig. 1(a). The difference in NSA was more easily appreciated when the water-to-fat ratio was closer to 1 [Figs. 1(b)–1(d) versus Figs. 4(b)–4(d)]. With the $(0,\theta,2\theta)$ encoding, θ is no longer limited to values close to π for a significant NSA when water and fat are similarly abundant.

Figure 4 also shows that for the LS estimation the lesser species (fat) did not always have a lower NSA than the more abundant species (water). For θ less than 0.55π, the NSA of fat was higher than that of water. This difference in NSA diminished as the water-to-fat ratio approached unity.

For both water and fat, the NSAs for the LS estimation were higher or equal to the NSAs for the analytic solution. The difference between these two estimations was dependent on the water-to-fat ratio and θ. This difference in NSA was

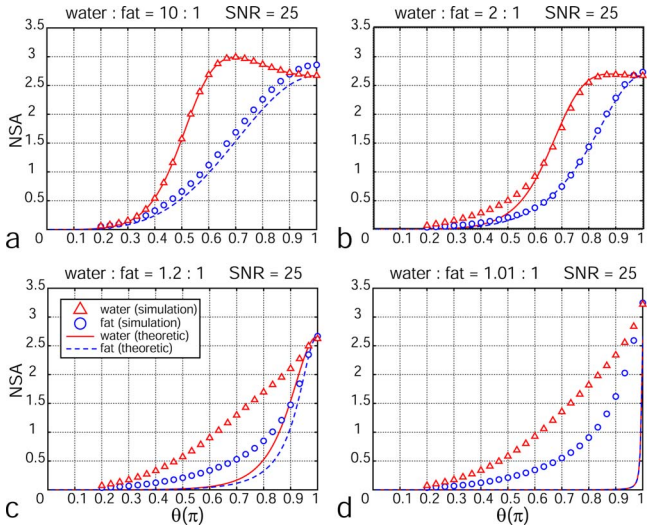

FIG. 5. Theoretically predicted NSA vs θ curves with Monte Carlo simulation results for MR signals with CS encoding of $(-\theta,0,\theta)$. The analytic solution was used to estimate water and fat. The water-to-fat ratios were (a) $R_{wf}=10$, (b) $R_{wf}=2$, (c) $R_{wf}=1.2$, and (d) $R_{wf}=1.01$. Data points of triangles and circles indicate NSAs for magnitudes of water and fat.

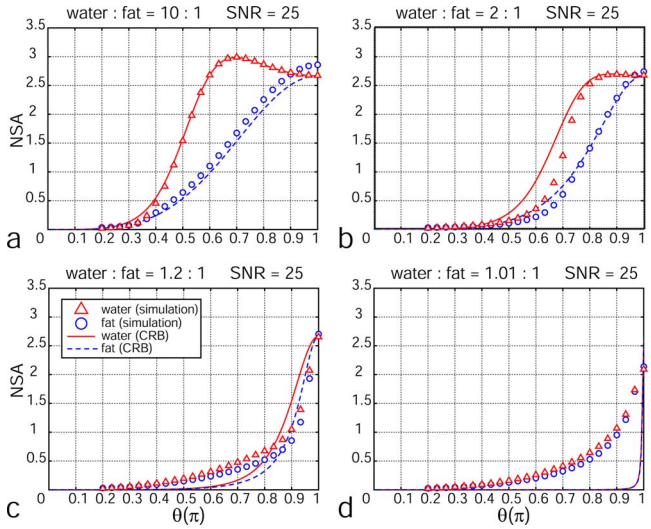

FIG. 6. NSA vs θ curves given by the CRB with Monte Carlo simulation results. MR signals were generated with the CS encoding of $(-\theta,0,\theta)$ and the LS solution was used to estimate water and fat. The water-to-fat ratios were (a) $R_{wf}=10$, (b) $R_{wf}=2$, and (c) $R_{wf}=1.2$, and (d) $R_{wf}=1.01$.

more pronounced for the lesser species when θ was between around 0.4π and 0.7π. The RMS errors (not shown here) of the LS estimation were lower or equal to the errors of the analytic solution, although the difference was not significant.

III.B. Low SNR simulation (SNR=25)

III.B.1. $(-\theta,0,\theta)$ *CS encoding*

With a lower SNR=25, similar simulations were performed to show how higher noise would affect the analytical and LS solutions. Figure 5 shows simulations similar to those shown in Fig. 1, except for a lower SNR at 25. With higher noise, the accuracy of the approximation of Eq. (9) can be affected. When water dominated fat, the effects were relatively minor [Figs. 5(a) and 5(b)]. With similar amounts of water and fat, Figs. 5(c) and 5(d) show that NSA of both water and fat were considerably higher than predicted with Eq. (9) because the approximation in Eq. (9) was no longer valid with large noise.

Figure 6 shows simulation results with a SNR of 25 and the same CS encoding as used in Fig. 2. For water-to-fat ratio of 10 [Fig. 6(a)], the water NSA matched the CRB well, while the fat NSA was slightly higher than the CRB. This is because the variance of the fat component (a small complex number) was reduced by taking its magnitude. For water-to-fat ratio of 2, noise effects appear for $\theta<0.8\pi$ [Fig. 6(b)]. The NSA from simulation became lower than the CRB, which could be caused by occasional erroneous swapping of water and fat due to lower SNR and small θ.

When water and fat components are close, swapping of water and fat may not substantially increase the variances of the estimates. Meanwhile, due to increased convergence to local minima and nonconvergence with a finite number of iterations, our implementation of LS fit may not represent a good MLE. In addition, the MLE may deviate from the CRB with a low SNR.[15] This NSA behavior can be seen in Fig. 6(d), which shows the NSA from simulation was in general higher than the CRB. In Fig. 6(c), deviation of simulation results from the CRB was more complicated due to mixed effects as exemplified in Figs. 6(b) and 6(d).

III.B.2. $(0,\theta,2\theta)$ *CS encoding*

Simulations were also performed with the $(0,\theta,2\theta)$ CS encoding at SNR=25. For the analytic method, simulation results were similar to those in Fig. 4 and they agreed well with theoretical predictions. For the LS method, excellent agreement between simulation and the CRB was observed for the dominant species (water), while minor deviation in NSA was occasionally found for the lesser species (fat).

III.C. Field map unknown versus field map known

When the noise is relatively high, field map smoothing as a way of regularization can be practiced to improve noise performance of water/fat separation. If the underlying field map is indeed smooth, extensive field map smoothing can potentially remove field map uncertainty, and the field map unknown problem becomes a field map known problem. Figure 7 shows the comparison between the CRB with a known field map and the CRB with an unknown field map when there was only one species ($R_{wf}=1:0$). With a known field map, the NSAs for water and fat were the same and only depended on the phase increment angle θ [see Eq. (17)]. When the field map was unknown, the NSA was calculated for two CS encodings: $(-\theta,0,\theta)$ and $(0,\theta,2\theta)$. The NSA curve for water remained the same for both encodings while the NSA curves for fat for the two encodings were different, resulting in different noise levels in the zero fat signal background.

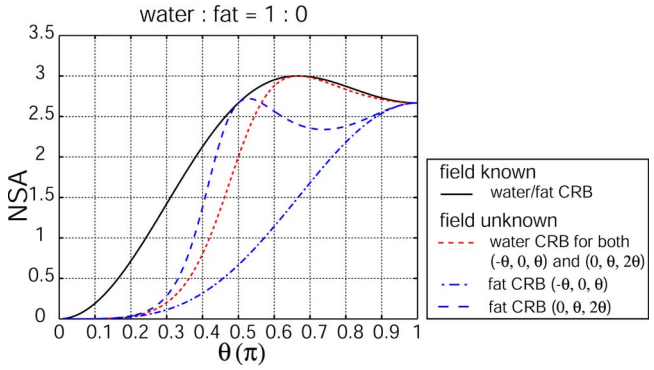

FIG. 7. Comparison of NSAs vs θ for the field-known and field-unknown cases. The CS encodings were $(-\theta,0,\theta)$ and $(0,\theta,2\theta)$ at $R_{wf}=1:0$. Note that the CRB for water remained the same while the CRB for fat was different for these two encodings.

In general the difference in NSA between the field map known and unknown is more significant for small θ, since in those cases the field map is more difficult to estimate. Researchers have explored how to reduce the impact to NSA from the error in the field map estimation. Field map smoothing was studied in Refs. 5 and 16 and the NSA performance of the field unknown problem was improved and was comparable to that when the field map is known. Nonetheless, field map smoothing requires that the true field map varies slowly in space. Otherwise, the smoothed field map may be significantly different from the true field map and thus introduce bias to the water and fat estimation. In practice, the type and size of the smoothing filter need to be carefully considered.

III.D. Geometric illustration of symmetric data acquisition

We have observed that with the symmetric $(-\theta,0,\theta)$ CS encoding and equal amounts of water and fat ($R_{wf}=1$), the NSAs of both water and fat were zero except for $\theta=\pi$. This NSA behavior can be seen with the analytic solution [Fig. 1 and Eqs. (11)] and the LS solution (Fig. 2). Here we will demonstrate that this phenomenon is not incidental and does not depend on the algorithm used to estimate ρ_w and ρ_f. As we show in the following, the NSAs are intrinsically zero because small noise in measured signals causes noise that is orders of magnitude higher in the estimated ρ_w and ρ_f.

When the water and fat signal magnitudes are equal or similar, the $(-\theta,0,\theta)$ encoding becomes problematic due to poor noise performance. When examined in the vector space, the signals are vector sums of the water and fat vectors at different relative phase angles (CS encoding angles). Estimating water and fat is an inverse problem with known water-fat phase difference at each echo time shift. When noise is present, the MR signals are altered in phase and magnitude, and the change in signals in turn affects the estimated water and fat. The NSA reflects how sensitively the estimated water and fat are influenced by the noise in the measured signals. The geometric configuration of the water and fat vectors at each echo time shift plays a role in linking the noise in the signals to the noise in estimated water and fat. If the change in the water and fat vectors can be quantified with respect to a given change in the MR signals, it would help explain the connection between the noise sensitivity of the water/fat estimation and the geometric MR signal configurations. Solving this inverse problem (water-fat separation) in a geometric way is not straightforward. However, analyzing how changes in ρ_w, ρ_f, and ϕ affect the MR signals can be demonstrated more easily in a geometric illustration. While it is difficult to derive a general theory that can account for any arbitrary case, a special example can help demonstrate how the geometric configurations of water and fat vectors can affect the noise performance of the water-fat separation method.

Figure 8(a) shows three MR signals $(\overrightarrow{OS}_{-1},\overrightarrow{OS}_0,\overrightarrow{OS}_1)$ represented by the sums of two rotating vectors (water $\boldsymbol{\rho}_w$ and fat $\boldsymbol{\rho}_f$), measured with the symmetric CS encoding $(-\theta,0,\theta)$. Vectors $\overrightarrow{OA}$ and $\overrightarrow{AS}_{-1}$ of lengths ρ_w and ρ_f, with an angle θ between them, represent the water and fat vectors at the first echo time shift, and they add to form signal $\overrightarrow{OS}_{-1}$. Water and fat are in-phase at the second echo $\overrightarrow{OS}_0$ and ϕ is the angle by which the water vector rotates due to the resonance offset. At the third echo, water and fat again form an angle θ for the signal $\overrightarrow{OS}_1$.

Let ρ_w, ρ_f, and ϕ be the correct solution. An alternative solution (with primed notation) can be determined as fol-

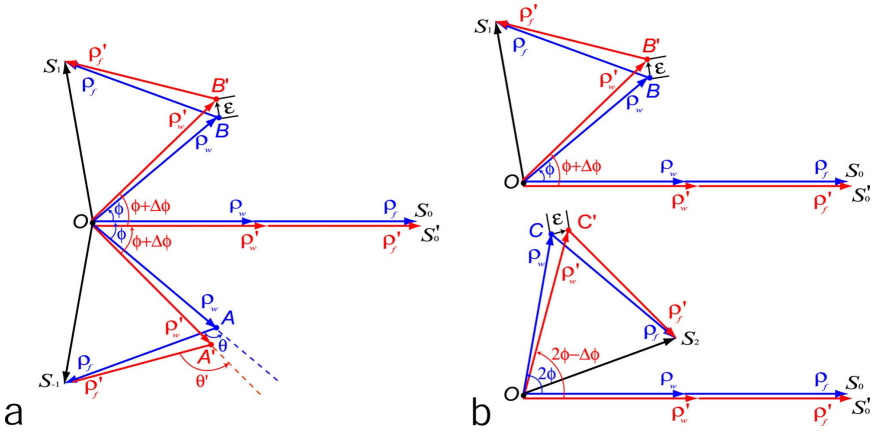

FIG. 8. Schematic of geometry for MR signals with the same amount of water and fat with the CS encoding scheme of (a) $(-\theta,0,\theta)$, and (b) $(0,\theta,2\theta)$. The plot at the top of (b) shows signals with CS encoding angles at 0 and θ, and the plot at the bottom of (b) shows signals with encoding angles at 0 and 2θ.

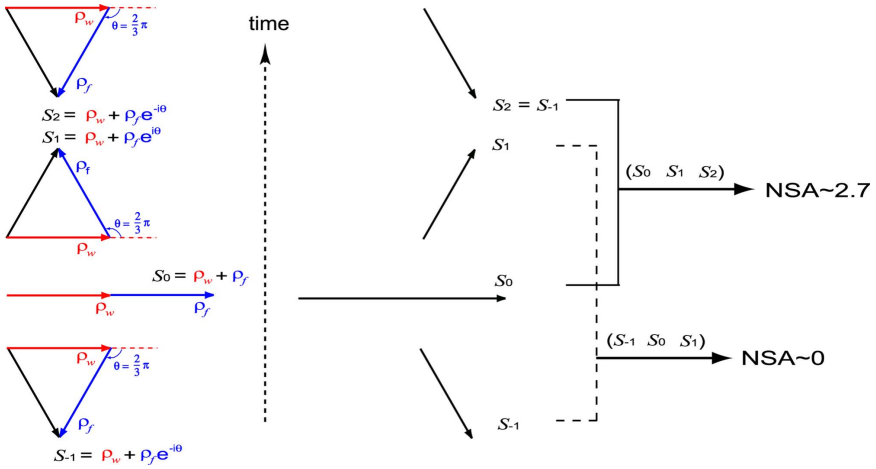

FIG. 9. Signals produced by equal amounts of water and fat at CS encoding of $(-\theta, 0, \theta, 2\theta)$.

lows. Move point B along the direction of $\overrightarrow{OS_1}$ by a small amount ε to obtain point B'. $\overrightarrow{OB'}$ and $\overrightarrow{B'S_1}$, of lengths ρ'_w and ρ'_f, respectively, are the new water and fat vectors for the third echo time shift and their vector sum is still S_1. Symmetrically, $\overrightarrow{OA'}$ and $\overrightarrow{A'S_{-1}}$ are the new water and fat vectors at the first echo time shift and they add to the same total MR signal S_{-1}. At the second echo, the water and fat vectors are aligned and form signal S'_0, differing from S_0 by $\Delta S'_0$. Since BB' is parallel to OS_1, $\angle OBS_1 = \angle OB'S_1 = \theta$ and the water-fat relative phase restriction is satisfied by the alternative solution. By geometry we have

$$\Delta\rho_w = \rho'_w - \rho_w = OB' - OB = \varepsilon \cos\frac{\theta}{2} + O(\varepsilon^2) = O(\varepsilon),$$

$$\Delta\rho_f = \rho'_f - \rho_f = B'S_1 - BS_1 = -\varepsilon \cos\frac{\theta}{2} + O(\varepsilon^2) = O(\varepsilon),$$

$$\Delta\phi = \frac{\varepsilon}{\rho_w}\sin\frac{\theta}{2}, \tag{19}$$

and consequently

$$\Delta S'_0 = OS'_0 - OS_0 = \rho'_w + \rho'_f - \rho_w - \rho_f = \Delta\rho_w + \Delta\rho_f = O(\varepsilon^2), \tag{20}$$

where $O(\varepsilon)$ is a small quantity of the same order as ε and $O(\varepsilon^2)$is a quantity of the order of ε^2. Thus, an $O(\varepsilon)$ change in the water and fat vectors results in a much smaller $O(\varepsilon^2)$ change in the measured signals. Conversely, a small $O(\varepsilon^2)$ change in the measured signal S_0 produces a much larger $O(\varepsilon)$ change in the computed water and fat magnitudes. That is to say, if the variance of the measured signals is $O(\varepsilon^2 \cdot \varepsilon^2)$, the variances of the water and fat estimates and the field map can be orders of magnitude higher, $O(\varepsilon \cdot \varepsilon)$. Their ratio, the NSA, is of $O(\varepsilon^2)$, practically zero in calculation. The above is the case until $\theta = \pi$ and Eqs. (19) become

$$\Delta\rho_w = \varepsilon \cos\frac{\theta}{2}\bigg|_{\theta=\pi} + O(\varepsilon^2) = O(\varepsilon^2),$$

$$\Delta\rho_f = -\varepsilon \cos\frac{\theta}{2}\bigg|_{\theta=\pi} + O(\varepsilon^2) = O(\varepsilon^2), \tag{21}$$

$$\Delta\phi = \frac{\varepsilon}{\rho_w}.$$

For $\theta = \pi$, i.e., the $(-\pi, 0, \pi)$ encoding, the NSAs for water and fat are finite but estimating the field map can be difficult. For voxels with equal amounts of water and fat, CS encodings in the form of $(-\theta, 0, \theta)$, except for $\theta = \pi$, should be avoided to have a good NSA performance.

With the CS encoding of $(0, \theta, 2\theta)$, as shown in Fig. 8(b), similar procedures were carried out to see if an alternative solution that does not change the signals could be found. In this case, a constant field map could not be achieved because the water vector progressed $\phi + \Delta\phi$ and $(2\phi - \Delta\phi) - (\phi + \Delta\phi) = \phi - 2\Delta\phi$ during the first and second intervals between MR signal acquisition. That is, the alternative solution is not physically realizable because it is not consistent with a constant off-resonance frequency. An alternative solution could not be found without changing the MR signals, and hence, variances of the estimates could not be orders higher than those of the signals.

An interesting paradox arises when $\theta = 2\pi/3$. The results above indicate that $(-2/3\pi, 0, 2/3\pi)$ and $(0, 2/3\pi, 4/3\pi)$ have dramatically different performances. However, $-2/3\pi$, and $4/3\pi$ are the same angle, so the two encoding schemes appear to differ only by an offset in time. We illustrate now how a difference can arise from two data sets of signals that seem to be numerically identical but different in time order.

Two vectors representing water and fat are shown in Fig. 9. Signals S_{-1}, S_0, S_1, and S_2 are acquired at four fat-water phase shifts of $(-2/3\pi, 0, 2/3\pi, 4/3\pi)$, with a zero offset frequency (unknown to the estimator). Signals S_{-1} and S_2 are the numerically identical. If S_{-1}, S_0, and S_1 are used to estimate ρ_w and ρ_f, the CS encoding is $(-\theta, 0, \theta)$ with $\theta = 2/3\pi$. The NSAs of water and fat are close to zero as has been described [Fig. 8(a)]. However, when S_0, S_1, and S_2 are used, the encoding becomes $(0, \theta, 2\theta)$. Even though it seems that the same set signals are collected in a different sequence, this

CS encoding does not have the symmetry that allows an alternative solution with a constant frequency offset. This signal configuration leaves no extra room for estimating the water and fat densities [Fig. 8(b)], resulting in a NSA of ~2.7.

IV. DISCUSSION

Our results indicate that the NSA of water-fat separation imaging is a complicated quantity that can be affected by many factors. When the field map is known, estimation of water and fat signals is a linear problem. Noise induced variations in the estimated water and fat are equal. The NSA is dependent on the CS incremental angle but not on the water-to-fat ratio or the initial CS encoding angle. For example, with a known field map the $(-\theta,0,\theta)$ and $(0,\theta,2\theta)$ CS encodings perform identically. When the field map is unknown, the field map becomes an unknown parameter to be estimated as well as the water and fat components. The noise in these parameters is correlated and parameter estimation is nonlinear. In addition to dependence of the CS incremental angle, the NSA also depends on the water-to-fat ratio and the NSA of water is usually different from that of fat if the amounts of water and fat are not the same. Comparison between the $(-\theta,0,\theta)$ and the $(0,\theta,2\theta)$ encodings shows that the initial CS encoding angle between water and fat can also affect the NSA. In general, the phase angle between water and fat at each of the three echo time shifts can be expressed as $(\theta_1,\theta_2,\theta_3)$. The NSA can be affected by each of these three encoding angles. In order to maximize the NSA, it is essential to optimize the combination of the three angles with different water to fat ratios.

When the SNR is high (>200), the LS solution consistently achieves the CRB regardless of the CS encoding. This is expected because the LS solution is the MLE for Gaussian noise, and the MLE can achieve the CRB asymptotically. Although the analytic solution is not a MLE, it achieves the CRB with CS encoding $(-\theta,0,\theta)$ at our computation precision. However, the analytic solution is not able to achieve the CRB with CS encoding $(0,\theta,2\theta)$. When the SNR is lower (~25), prediction of noise performance may not be as accurate for both solutions. This is especially true for the $(-\theta,0,\theta)$ encoding. Nonetheless, the $(0,\theta,2\theta)$ seems to be less affected by large noise.

Calculating CRB directly is a fast way to predict the noise performance of algorithms that could achieve the CRB asymptotically. However, the actual noise performance can be affected by the SNR and the implementation of the algorithm. The CRB can be used to guide optimization of the imaging parameters such as the CS encoding angles, and Monte Carlo simulations may give more accurate predictions of the noise performance.

With low SNR data, regularization (such as field map smoothing) can be employed to reduce the variance of the estimation at the risk of potentially introducing bias. Tradeoffs between variance and bias can be explored to fit the needs of specific clinical applications.

V. CONCLUSIONS

The noise performance of the three-point water-fat separation method with an unknown field map is dependent on the water to fat ratio and the angle between water and fat at every echo time shift. Various estimation algorithms may have different noise performances. At high SNR, the LS solution is able to achieve the CRB. The analytic solution performs just as well with the $(-\theta,0,\theta)$ CS encoding, while it underperforms the LS solution with the $(0,\theta,2\theta)$ CS encoding. Low SNR data can cause the noise performance of both solutions to deviate from theoretic predictions, especially for the $(-\theta,0,\theta)$ CS encoding. This symmetric CS encoding scheme (except for $\theta=\pi$) causes intrinsic difficulty when fat and water are present in equal amounts. We provide a geometric explanation for this behavior. Monte Carlo simulation can be helpful to provide more accurate predictions for water-fat separation in practice.

ACKNOWLEDGMENTS

This work was supported by NIH Grant No. RR09784, GE Healthcare, and the Lucas Foundation. The authors gratefully acknowledge helpful discussion with Dr. Huanzhou Yu.

[a]Current address: Department of Medical Physics, University of Wisconsin-Madison, Madison, WI 53792. Electronic mail: wenzf@stanfordalumni.org
[b]Current address: Department of Radiology, University of Wisconsin-Madison, Madison, WI 53792.
[c]Current address: Department of Mathematics, California State University, Fullerton, CA 92834.

[1]W. T. Dixon, "Simple proton spectroscopic imaging," Radiology **153**, 189–194 (1984).
[2]G. H. Glover and E. Schneider, "Three-point Dixon technique for true water/fat decomposition with B0 inhomogeneity correction," Magn. Reson. Med. **18**, 371–383 (1991).
[3]G. H. Glover, "Multipoint Dixon technique for water and fat proton and susceptibility imaging," J. Magn. Reson. Imaging **1**, 521–530 (1991).
[4]J. Ma, S. K. Singh, A. J. Kumar, N. E. Leeds, and L. D. Broemeling, "Method for efficient fast spin echo Dixon imaging," Magn. Reson. Med. **48**, 1021–1027 (2002).
[5]Q. S. Xiang and L. An, "Water-fat imaging with direct phase encoding," J. Magn. Reson. Imaging **7**, 1002–1015 (1997).
[6]S. B. Reeder, Z. Wen, H. Yu, A. R. Pineda, G. E. Gold, M. Markl, and N. J. Pelc, "Multicoil Dixon chemical species separation with an iterative least-squares estimation method," Magn. Reson. Med. **51**, 35–45 (2004).
[7]Q. Chen, E. Schneider, B. Aghazadeh, M. S. Weinhous, J. Humm, and D. Ballon, "An automated iterative algorithm for water and fat decomposition in three-point Dixon magnetic resonance imaging," Med. Phys. **26**, 2341–2347 (1999).
[8]S. Chavez, Q. S. Xiang, and L. An, "Understanding phase maps in MRI: A new cutline phase unwrapping method," IEEE Trans. Med. Imaging **21**, 966–977 (2002).
[9]E. R. McVeigh, R. M. Henkelman, and M. J. Bronskill, "Noise and filtration in magnetic resonance imaging," Med. Phys. **12**, 586–591 (1985).
[10]A. R. Pineda, S. B. Reeder, Z. Wen, and N. J. Pelc, "Cramer–Rao bounds for three-point decomposition of water and fat," Magn. Reson. Med. **54**, 625–635 (2005).
[11]S. B. Reeder, A. R. Pineda, Z. Wen, A. Shimakawa, H. Yu, J. H. Brittain, G. E. Gold, C. F. Beaulieu, and N. J. Pelc, "Iterative decomposition of water and fat with echo asymmetry and least-squares estimation (IDEAL): Application with fast spin-echo imaging," Magn. Reson. Med. **54**, 636–644 (2005).
[12]H. Yu, S. B. Reeder, A. Shimakawa, J. H. Brittain, and N. J. Pelc, "Field map estimation with a region growing scheme for iterative 3-point water-fat decomposition," Magn. Reson. Med. **54**, 1032–1039 (2005).
[13]H. Yu, S. B. Reeder, A. Shimakawa, J. H. Brittain, and N. J. Pelc, "Ro-

bust field map estimation in a Dixon water-fat separation algorithm with short echo time increments," Proceedings of the International Society Magn. Reson. Med., 12th Annual Meeting, 2004, p. 345.
[14]H. L. Van Trees, *Detection, Estimation, and Modulation Theory* (Wiley, New York, 1968).
[15]S. P. Muller, C. K. Abbey, F. J. Rybicki, S. C. Moore, and M. F. Kijewski, "Measures of performance in nonlinear estimation tasks: Prediction of estimation performance at low signal-to-noise ratio," Phys. Med. Biol. **50**, 3697–3715 (2005).
[16]Q. S. Xiang, "Two-point water-fat imaging with partially-opposed-phase (POP) acquisition: An asymmetric Dixon method," Magn. Reson. Med. **56**, 572–584 (2006).